BIOCYBERNETICS AND BIOMEDICAL ENGINEERING 42 (2022) 437–452

Available at www.sciencedirect.com

ScienceDirect

journal homepage: www.elsevier.com/locate/bbe

Original Research Article

Fourier transform-based data augmentation in deep learning for diabetic foot thermograph classification

Andrés Anaya-Isaza [a,b,*], *Martha Zequera-Diaz* [a]

[a] *Electronics Department, BASPI - FootLab, Pontificia Universidad Javeriana, Bogotá, Colombia*
[b] *INDIGO Research, Bogotá, Colombia*

ARTICLE INFO

Article history:
Received 14 October 2021
Received in revised form
1 March 2022
Accepted 1 March 2022
Available online 8 March 2022

Keywords:
Artificial intelligence
Computational and artificial intelligence
Diabetes
Image classification
Machine learning
Medical diagnostic imaging

ABSTRACT

Diabetes Mellitus (DM) belongs to the ten diseases group with the highest mortality rate globally, with an estimated 578 million cases by 2030, according to the World Health Organization (WHO). The disease manifests itself through different disorders, where vasculopathy shows a chronic relationship with diabetic ulceration events in distal extremities, being temperature a biomarker that can quantify the risk scale. According to the above, an analysis is performed with standing thermography images, finding temperature patterns that do not follow a particular distribution in patients with DM. Therefore, the modern medical literature has taken the use of Computer-Aided Diagnosis (CAD) systems as a plausible option to increase medical analysis capabilities. In this sense, we proposed to study three state-of-the-art deep learning (DL) architectures, experimenting with convolutional, residual, and attention (Transformers) approaches to classify subjects with DM from diabetic foot thermography images. The models were trained under three conditions of data augmentation. A novel method based on modifying the images through the change of the amplitude in the Fourier Transform is proposed, being the first work to perform such synergy in the characterization of risk in ulcers through thermographies. The results show that the proposed method allowed reaching the highest values, reaching a perfect classification through the convolutional neural network ResNet50v2, promising for limited data sets in thermal pattern classification problems.

© 2022 The Author(s). Published by Elsevier B.V. on behalf of Nalecz Institute of Biocybernetics and Biomedical Engineering of the Polish Academy of Sciences. This is an open access article under the CC BY-NC-ND license (http://creativecommons.org/licenses/by-nc-nd/4.0/).

1. Introduction

The epidemiology of diabetes mellitus (DM) shows alarming statistics worldwide. According to the International Diabetes Federation (IDF), type 1 and 2 DM prevalence increased from 151 million to 463 million between 2000 and 2019 [1]. The IDF classifies the pathology as a pandemic, placing it among the ten leading causes of mortality worldwide, where 578

* Corresponding author at: Pontificia Universidad Javeriana, 110231 Bogotá, Colombia.
E-mail addresses: anayaandresj@javeriana.edu.co (A. Anaya-Isaza), mzequera@javeriana.edu.co (M. Zequera-Diaz).
https://doi.org/10.1016/j.bbe.2022.03.001
0168-8227/© 2022 The Author(s). Published by Elsevier B.V. on behalf of Nalecz Institute of Biocybernetics and Biomedical Engineering of the Polish Academy of Sciences.
This is an open access article under the CC BY-NC-ND license (http://creativecommons.org/licenses/by-nc-nd/4.0/).

million people with DM are expected by 2030 [1,2]. Furthermore, it is estimated that this figure will reach 700 million by 2045 (10.9% of the world population) [1].

On the other hand, the reported health expenditure related to DM was significant and estimated at US$ 69.7 billion. The value evidences a proportion of 9.2% of the world total. Therefore, investment in complementary treatments for DM is expected to increase from 15.3% in 2030 to 22.9% in 2045, equivalent to USD 85.7 billion, to address this metabolic catastrophe and mitigate its detrimental impact on the individual and society [1,3,4].

DM leads to a group of metabolic disorders due to total or partial deficiency of the polypeptide hormone insulin [5]. This hormone is responsible for regulating blood sugar levels, where the uncontrolled effect of DM results in hyperglycemia [2]. Macrovascular complications of type 1 and 2 DM, such as peripheral arterial disease, myocardial infarction, and stroke, among others, prediabetic evidence stages [6]. The most common pattern of diabetic complications is expressed in cardiovascular diseases (CVD) such as coronary artery disease, peripheral arterial disease, and cerebrovascular diseases that produce deaths, hospitalizations, procedures for acute coronary syndromes, myocardial infarction, sudden death, as well as ischemic and hemorrhagic stroke, are the leading causes of mortality and morbidity in diabetic patients [7,8]. It is stated that peripheral artery disease is the main cause of amputations in the lower extremities and that one-third of all deaths are due to CVD [9].

Another of the most frequent chronic complications of type 2 DM is vasculopathy [10], this condition evidences pathogenesis of ulceration in the distal extremities –known as neuroischemic foot– related to severe chronic complications such as diabetic foot syndrome [10,11]. The pathophysiology of the diabetic foot evidences a set of disorders such as loss of proprioception, decreased temperature perception, vibration perception deficit, and biomechanical alterations of the foot [12,13]. This can lead to polytraumatic events or vascular disorders, causing tissue breakdown due to increased temperature caused by the pressure-friction relationship, generating the subcutaneous eruption that finally triggers a chronic diabetic ulcer [14]. Ulceration in the lower limbs is known as diabetic foot and has a high risk of becoming infected, limiting the healing time or making it difficult to reduce the progression of these conditions [15]. Even in the worst-case scenario, the lower limbs must be amputated to prevent the progression of ulcerations and infections [16]. In fact, in Europe, 250 thousand patients underwent this type of surgical intervention, and in the United States, this figure is approximately 1 million interventions per year [17,18]. Under the above, several authors such as David Armstrong, Andrew Boulton, and Sicco Bus [19–21] conducted a systematic review of the phenomenon of diabetic ulceration, where Peripheral Arterial Disease (Vasculopathy) and Loss of Protective Sensation (Neuropathy) are related, concluding that the risk of ulceration on the plantar surface correlates directly with shear (pressure plus friction) [22]. However, this variable is difficult to measure [23–26], which has led to taking temperature as a predictive biomarker, according to Metin Yavuz et al. [27].

Even the plantar temperature of the diabetic foot has motivated the development and implementation of new technologies for the early detection of temperature alterations associated with ulceration risk. In this regard, infrared (IR) cameras have been included to map the correlation of maximum temperature and diabetic neuropathic foot [28,29]. The technique allows rapid capture of the plantar thermal distribution [30]. Furthermore, in medicine, this tool is widely used to identify vascular disorders [31,32] and for the detection of diabetes (See related work section).

The recent inclusion of infrared thermal imaging has increased computer-aided diagnosis (CAD) capacity, obtaining reliable and efficient measurements [33]. The scientific community continues to develop this technology, where every day, new techniques or methods emerge to improve CAD systems [34]. Many of these approaches are part of machine learning (ML) or deep learning (DL), a topic of exponential growth in medical informatics [35]. DL has shown better performance than ML in pattern recognition, segmentation, registration, characterization, and classification [36]. It is even possible to find deep learning algorithms that have outperformed human performance [37].

Following the above considerations, this paper proposes implementing three deep learning architectures for the classification of healthy subjects (control group) and subjects with diabetes through foot thermographs. The architectures are based on three of the best approaches reported in state-of-the-art, i.e., a convolutional neural network, a residual, and a transformer were considered. The development aims to identify subjects with DM before they manifest diabetic foot disorder, resulting in avoiding subsequent ulcerations on the sole. Additionally, a novel data augmentation technique based on image modification through variations in the amplitude derived from the Fourier transform is also proposed due to limited databases.

2. Related work

New image processing techniques and developments in artificial intelligence have opened up new possibilities in computer-aided diagnosis (CAD). Research shows significant advances in the detection, classification, prediction, and segmentation of medical images [38]. Algorithms provide various tools for accurate diagnosis, reducing errors due to negligence, fatigue, information overload, or limitations of human perception [39,40]. In this way, several tools and techniques have been developed to classify subjects with diabetic foot, where recent studies have proposed algorithms from basic techniques in image processing or analysis to novel deep learning methods based on attention or self-learning. For example, Adam et al. [41] conducted a review of CAD systems. They stated that the study of diabetic foot is mainly classified into four types: independent lower extremity temperature analysis, asymmetric temperature, temperature distribution, and thermal and physical stress analysis.

Mori et al. [42] addressed the search for morphological patterns in temperature distribution. Subjects with DM showed a full-high pattern with a recurrence of 46%, followed by the butterfly pattern (12%). In the control group, the butterfly pattern was more frequent (44%) than the full-high pattern (19%).

Liu et al. [43] looked for asymmetric patterns between both feet. They approached the process by segmenting and record-

ing the two feet in the same image space. Subsequently, they calculated the thermal difference between the images and set a temperature threshold of 2.2 °C, generating risk zones associated with DM subjects. Adam et al. [44] implemented a support vector machine (SVM) to classify DM subjects in a more robust approach. The development was based on discrete wavelet transform (DWT), higher-order spectra (HOS), texture, and entropy, to generate the training techniques features of the SVM. In this case, the classification achieved an accuracy of 89.39%, a sensitivity of 81.81%, and a specificity of 96.97%. Similarly, Carlos Padierna et al. [45] and Selle et al. [46] used the SVM algorithm. The former used the SVM to classify peripheral arterial disease through thermography from the top of the foot. The trials achieved 92.64, 91.80, and 93.59% in accuracy, sensitivity, and specificity metrics. The latter used gray level textures features as inputs for SVM, achieving an accuracy of 96.42%. For his part, Hernandez et al. [47] employed machine learning techniques in the same vein, using a multilayer perceptron (MLP) architecture. Hernandez used a segmentation process to obtain the highest temperature region and generated a feature vector from the pattern spectrum technique, achieving a classification rate of 94.33%. Finally, in the most recent study, Cruz et al. [48] developed a deep learning network called DFTNet, after analyzing an SVM, an MLP, and the AlexNet and GoogLeNet architectures. The development reported the highest classification values so far, where 97.83, 100, and 95.83% were reached in accuracy, sensitivity, and specificity metrics, respectively. Finally, Khandakar et al. used several approaches, from machine learning strategies with feature extraction to state-of-the-art deep learning convolutional networks. The research compared the different methods, achieving an F1 score of 97%. In addition, the thermographic images were enhanced with strategies such as histogram equalization, adaptive histogram equalization, and gamma correction [49].

While the results are promising and DL are evolving rapidly, some limitations restrict the implementation of these algorithms. For example, one of the most common limitations is the restricted access to a large corpus of data [50]. Networks need to adjust the hundreds or thousands of model parameters to converge to an accurate classification. In this regard, studies and research with diabetic foot thermographs have lagged behind because of the limited availability of labeled data. Not surprisingly, at publishers such as Elsevier, the two most recent investigations are from the 2020s and 2021. In fact, the most relevant publications do not go beyond a couple of articles per year, as shown in Table 1.

The compilation of the articles shown in Table 1 again confirms the need to include new data enhancement strategies.

3. Materials and methods

3.1. Data set

The experiment was performed on the public database "Plantar Thermogram Database for the Study of Diabetic Foot Complications" [51]. The database has two sets of thermal images of the foot sole (thermograms). The first is a set of 122 subjects diagnosed with diabetes, and the second is a group of 45 control subjects, i.e., non-diabetic subjects or control group (CG). Each subject has the right and left foot images in .csv files, where the actual temperature in degrees Celsius is recorded.

The files were used to create the foot images by taking the temperature values located in each file's different rows and columns, which corresponded to the real spatial positions of the images (Grayscale image). In addition, 80% of the data were randomly taken for training. The remaining 20% was used for validation during training and post-training testing by taking equal parts in these two data sets, i.e., 10% in each set.

3.2. Preprocessing

Deep learning techniques are characterized by working with raw data [52]. Therefore, only three basic preprocessing steps were performed. First, the grayscale images were transformed to RGB, replicating the intensity levels in the three RGB channels. Second, the images were adjusted to 199×88 dimensions, as they were not all the same size. That is, images with sizes smaller than 199×88 had the corresponding rows and columns added to complete that size (Rows and columns of zeros). Finally, the images were normalized concerning the maximum and minimum of the data set, i.e., temperatures 15.98–37.28 °C took the values from 0 to 1.

3.3. Data augmentation

In the last decade, the effectiveness of deep learning neural networks has been more than demonstrated throughout the literature and research [53]. However, although the results are promising, most authors state one of the main problems related to DL algorithms. The methods generalize with high accuracy but require large amounts of data to train the hundreds or thousands of internal model parameters [54]. The most obvious solution is to have a large corpus of data; however, this is not possible in medicine due to: the high costs in the acquisition of medical images, the low frequency of some pathologies, the few images with descriptions (labels), and even the reduced platforms that centralize the information to distribute them freely. In this order of ideas, the limited data sets have motivated the synthesis of artificial images through different strategies, among which is mainly data augmentation. The method consists of taking a reference image and creating new images by performing various transformations. The most common and widely used examples are the geometric transformations of rotation or flipping [55]. Based on the above considerations, we chose to use data flipping (see Fig. 1), and a new technique based on the Fourier transform described in detail in the next section.

3.4. Fourier data augmentation

The Fourier transform is a mathematical transformation used to convert a signal from time (or space) to frequency domain. The process is mathematically defined as follows:

$$X_{k_1,k_2} = \sum_{n=0}^{R-1} \sum_{m=0}^{C-1} x_{n,m} e^{-2\pi i \left(\frac{k_1 n}{R} + \frac{k_2 m}{C}\right)} \quad (1)$$

Table 1 – Most recent and relevant research related to thermography of the foot in diabetic subjects.

Year	Authors	Title	Number of subjects	Data augmentation	Topic	Metric scores (%)
2021	A. Khandakar [49]	A machine learning model for early detection of diabetic foot using thermogram images.*	122 DM and 45 CG	Image rotation and translation	ML and DL	F1 score 97
2021	J. Josephine Selle [46]	Classification of Foot Thermograms using Texture Features and Support Vector Machine.	25 DM and 25 CG	None	ML	Accuracy 96.42
2020	L. Padierna [45]	Classification method of peripheral arterial disease in patients with type 2 diabetes mellitus by infrared thermography and machine learning.*	23 DM and 20 CG	None	ML	Accuracy 92.64, sensitivity 91.80, and specificity 93.59.
2020	I. Cruz-Vega [48]	Deep Learning Classification for Diabetic Foot Thermograms.	122 DM and 45 CG	Image rotation and flipping.	ML and DL	Sensitivity 91.67 and accuracy 85.3
2018	M. Adam [44]	Automated characterization of diabetic foot using nonlinear features extracted from thermograms.*	33 DM and 33 CG	None	ML	Accuracy 89.39, sensitivity 81.81 and specificity 96.97
2015	C. Liu [43]	Automatic detection of diabetic foot complications with infrared thermography by asymmetric analysis.	76 DM	None	IP	Sensitivity 97.8 and specificity 98.4
2015	D. Hernandez-Contreras [47]	Automatic classification of thermal patterns in diabetic foot based on morphological pattern spectrum.*	30 DM and 30 CG	None	IP and ML	Sensitivity 97.33, specificity 91.33 and precision 92.24
2013	T. Mori [42]	Morphological Pattern Classification System for Plantar Thermography of Patients with Diabetes.	129 DM and 32 CG	None	IP	There are no classification metrics

ML: Machine learning, DL: Deep Learning and IP: Image processing.
* Articles from Elsevier journals.

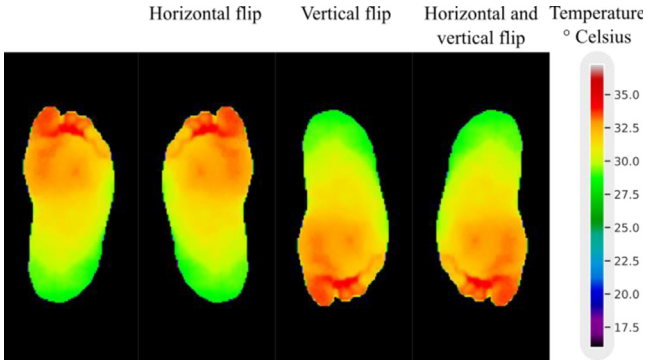


Fig. 1 – Example of data augmentation through image flipping.

$k_1 = 0, \cdots, R-1$

$k_2 = 0, \cdots, C-1$

Eq.ation (1) is the discrete Fourier transform for a two-dimensional signal, where R and C are the sizes on the y and x-axes. The variable i is the imaginary unit, and k_1 y k_2 represent the k-th signal values indices in the frequency domain.

Because of the imaginary unit in the exponent, the Fourier transform generates complex results. Therefore, it is possible to represent the result (X_{k_1,k_2}), in its magnitude and phase, as shown in Eqs. (2) and (3).

$$A_{k_1,k_2} = \sqrt{Re(X_{k_1,k_2})^2 + Im(X_{k_1,k_2})^2} \tag{2}$$

$$\varphi_{k_1,k_2} = arctan\left(\frac{Im(X_{k_1,k_2})}{Re(X_{k_1,k_2})}\right) \tag{3}$$

Here, *Re* and *Im* are the real and imaginary parts of the complex values. The real part indicates the proportion associated with each sinusoidal component (X_{k_1,k_2}) in the image, and the phase indicates each component's position. Therefore, if the amplitude is modified, the image would retain the spatial distribution when applying the inverse Fourier transform. The following mathematical expression governs the inverse process:

$$x_{n,m} = \frac{1}{RC}\sum_{k_1=0}^{R-1}\sum_{k_2=0}^{C-1} X_{k_1,k_2} e^{2\pi i\left(\frac{k_1 n}{R}+\frac{k_2 m}{C}\right)} \tag{4}$$

Following this principle, it is proposed to partially alter the amplitude to generate variations in the image while preserving the spatial distribution.

The amplitude variation in the Fourier transform was performed by generating a random image of the same size as the amplitude matrix in Fourier transform, with values from 0 to 1 and with uniform distribution (called noise image). Subsequently, the Hadamard product was performed between the amplitude and the noise, generating a matrix with modified amplitude. Finally, the inverse Fourier transform was performed with this amplitude and the original phase to obtain the image again in the space domain (Eq. (4)). Fig. 2 shows a practical example of this process.

3.5. *Artificial neural networks*

Artificial neural networks (ANNs) are one of the first bio-inspired systems based on the functioning of the human brain. In particular, the brain can perform complex cognitive tasks generated through the interaction of millions of neurons. Neurons receive electrochemical signals from other neurons or signals generated by the different tissues that make up our senses, such as vision. Each neuron processes the signals and depending on the interactions with the other neurons, these can reach the action potential, polarizing the neuron's axon that allows the electrical signal transmission (Action known as synapse). The process can be emulated in artificial neural networks by exchanging the biological neuron

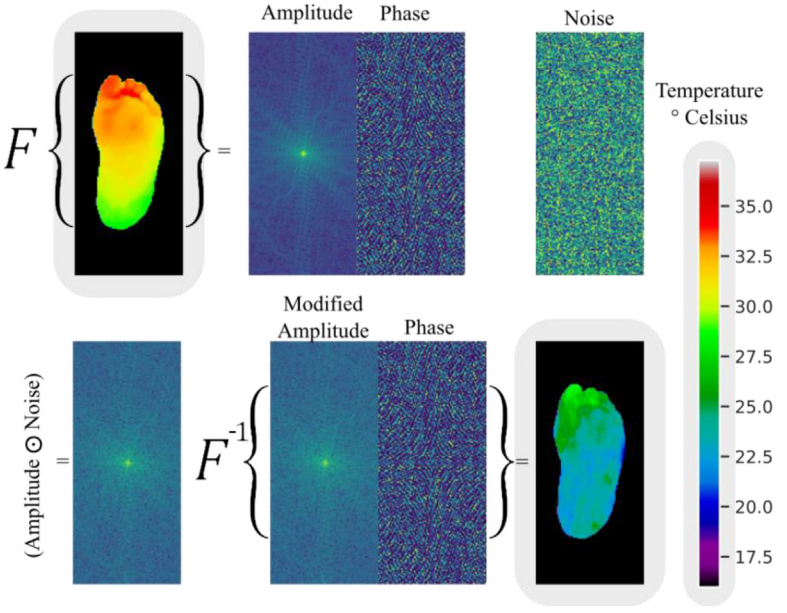


Fig. 2 – Example of data augmentation through Fourier transform in thermographic images.

for an artificial neuron, governed by a mathematical model as expressed in Eq. (5).

$$y = \varphi\left(b + \sum_{i=0}^{n} w_i x_i\right) \tag{5}$$

Here, x is the model inputs, w is the vector of weights that simulates the synaptic weights of the electrochemical interactions. $\sum$ is the total cumulus of all interactions. b is the bias that modifies the action potential threshold, and φ is the activation function, i.e., the activation generated by axon polarization in the case of the biological neuron. Eq. (5) is the simplest model of neural networks. However, the model's potential is reached when the network is constructed with several layers and several neuronal units per layer.[56,57].

As mentioned above, deep learning architectures are techniques that have proven to be highly efficient, outperforming conventional machine learning techniques. Therefore, it was proposed to implement 3 of the state-of-the-art architectures for thermogram classification. The first model is ResNet50v2, which consists of convolutional layers in sequence. The architecture increases the number of filters in each layer and, in turn, reduces the image size at each step. The second model implements the new technique known as Transformers. The architecture follows the same sequence of layers by reducing the data's dimension to obtain the features to classify the images. However, unlike the first model, this one changes the convolutional layers by Transformers blocks, i.e., layers with attention systems. Finally, in a recent study, the network known as DFTNet was created, designed for the specific classification of thermographic images of diabetic foot. Table 2 summarizes some of the main characteristics of the architectures; however, the models are made available to the public in the following Github repository. (https://github.com/AndresAnayaIsaza/FourierDeepLearningFoot/). Additionally, the models are described in more detail in the next section.

3.6. *DFTNet*

Although convolutional neural networks became known from LeCun et al. [58], it was not until the AlexNet network won the "ImageNet 2012 Large Scale Visual Recognition Challenge" that the computer vision paradigm was changed. The network demonstrated that features obtained through DL could outperform manually designed features used in conventional machine learning methods [59]. The network is the reference for most convolutional architectures, such as the DFTNet network, devised to classify standing thermographs [48]. The architecture does not differ much from AlexNet. It consists of 5 convolutional layers with 32, 64, 64, 64, 32, and 32 filters. The network has Batch-Normalization layers after four of the five convolutional layers and has three clustering layers (MaxPooling). In addition, the architecture has a fully connected layer that converges to two outputs corresponding to the two classes (CG and DM). The convolutional model is similar to Eq. (5), but the summation argument is changed by the convolutional product between the input image and the filter, as expressed in Eq. (6).

$$A_j = \varphi\left(b_j + \sum_{i=1}^{M} X_i * K_{ij}\right) \tag{6}$$

Here, X_i is the input image in the i-th channel (3 channels for an RGB image), K_{ij} is the i-th channel of the j-th filter. b_j is the bias associated with the j-th filter, φ is the activation function, and A_j is the map generated by the j-th filter. The process is repeated through all layers, causing the input image to progress through the different convolutional layers generating more abstract feature maps. In other words, the model in Eq. (6) can be generalized for any layer, as expressed in Eq. (7).

$$A_j^{(l)} = \varphi^{(l)}\left(b_j^{(l)} + \sum_{i=1}^{M^{(l-1)}} A_i^{(l-1)} * K_{ij}^{(l)}\right) \tag{7}$$

where the superscript (l) represents the l-th layer, and the input image is changed by the output feature maps of the previous layer.

3.7. *ResNet50v2*

As mentioned above, DL networks are characterized by creating abstract feature maps that converge to an output corresponding to the desired task. That is, networks are a type of hierarchical algorithm that depends on a series of layers. Research has shown that the increasing number of layers makes it possible to tackle more complex problems. However, the depth limits the network's training due to gradient fading, i.e., since the gradient propagates backward between different layers, repeated multiplication over many layers makes the gradient too small. To solve this problem, He et al. introduced the concept of residual connection or direct connection [60]. Essentially, the connection creates parallel paths to the convolutional layer sequences, causing the gradient to flow through the layers and preventing the gradient from shrinking. The connection forces the network to learn the residual mapping $f(x) - x$, which is easier to train when the residual mapping has the form of the identity function $f(x) = x$ [61].

Parallel connections are added to the model every three convolutional layers, as expressed in Eqs. (8) and (9).

Table 2 – Summary of architectures.

Models	Convolutional layers	Number of filters	Training parameters
DFTNet	5	224	85,378
ResNet50v2	53	26,560	23,523,458
Transformer	8*	64**	23,770,953

* Multi-head Attention with 4 attention heads.
** Dimensions of the projection.

$$A_j^{(R)} = \varphi^{(l)}\left(b_j^{(l)} + \sum_{i=1}^{M^{(l-1)}} A_i^{(l-1)} * K_{ij}^{(l)}\right) + \varphi^{(R)}\left(b_j^{(R)} + \sum_{i=1}^{M^{(l-3)}} A_i^{(l-3)} * K_{ij}^{(R)}\right) \quad (8)$$

$$A_j^{(R)} = \varphi^{(l)}\left(b_j^{(l)} + \sum_{i=1}^{M^{(l-1)}} A_i^{(l-1)} * K_{ij}^{(l)}\right) + \varphi^{(R)}\left(b_j^{(R)} + \sum_{i=1}^{M^{(R-1)}} A_i^{(R-1)} * K_{ij}^{(R)}\right) \quad (9)$$

Here, the term on the right-hand side of Eq. (8) is the output of the after antepenultimate layer or the output of the previous residual block (see Eq. (9)) [60].

3.8. Transformer

The Transformer is one of the newer architectures that does not rely on convolutional and recurrent layers. In fact, transforms are changing the way deep learning algorithms are implemented. The architecture is based on the concept of attention mechanisms that allow information to be abstracted at the points of most significant relevance, i.e., "paying attention" to relevant information. Mathematically, Transformers is based on the attention model expressed in Eq. (10) [62].

$$Head_i = softmax\left(\frac{Q_i K_i^T}{\sqrt{d_k}}\right) V_i \quad (10)$$

The model in Eq. (10) makes part of a series of headers that can vary at the choice of the architecture design. In the equation, Q_i, K_i, and V_i are the queries, keys, and values of the care model, which are generated by the following equations:

$$Q_i = xW_i^q W_i^q \in \mathbb{R}^{d\times d_q} \quad (11)$$

$$K_i = xW_i^k W_i^k \in \mathbb{R}^{d\times d_k} \quad (12)$$

$$V_i = xW_i^v W_i^k \in \mathbb{R}^{d\times d_v} \quad (13)$$

where the W matrices are the Transformers weights matrices, which are determined through model training [62].

3.9. Loss function

The models were trained through the cross-entropy (CE) loss function, allowing to classify the output in probability values between values from 0 to 1. The CE takes the following mathematical form for the case of n observations and two classes.

$$CE = -\sum_{i=0}^{n} y_i log(\hat{y}_i) + (1 - y_i) log(1 - \hat{y}_i) \quad (14)$$

where y_i and $\hat{y}_i$ are the i-th real and predicted observations, respectively.

3.10. Evaluation metrics

As an essential part of an objective comparison of the models used, the proposed approach was based on four different evaluation metrics: Accuracy, sensitivity, specificity, and false-positive rate (*FPR*). The four metrics are mathematically expressed as follows:

$$Accuracy = \frac{TP + TN}{TN + TP + FP + FN} \quad (15)$$

$$Sensitivity = \frac{TP}{TP + FN} \quad (16)$$

$$Specificity = \frac{TN}{TN + FP} \quad (17)$$

$$FPR = \frac{FP}{TP + FP} \quad (18)$$

The three metrics are established in terms of true positives (*TP*), true negatives (*TN*), false positives (*FP*) and false negatives (*FN*).

3.11. Experiments

The three deep learning models were trained with the database in its four configurations, i.e., without data augmentation, image flipping, Fourier imaging, and combined these two data augmentation techniques. The process was performed with all feet separately, i.e., the feet of each subject were taken as independent data. In addition, the data augmentation was proportional to the amount of data per type (Controls and Diabetics).

Although the data are in an approximate ratio of 3 to 1, each base image was increased by the same amount. However, anticipating bias due to unbalanced data, we chose to use different metrics; sensitivity to determine the proportion of positives (diabetics) and specificity to determine the proportion of negatives (controls).

Fig. 3 shows the general description of the algorithm used in the last case. The code takes the thermographic images and delivers the model for automatic classification. Initially, the images are normalized and divided into three data sets: training, validation, and test. The training data is flipped on the two axes and added to the original images. Subsequently, each image is Fourier transformed to calculate the amplitude and phase in frequency space. The amplitude is multiplied (Hadamard product) with the random noise, generating the new amplitude. The original phase and modified amplitude are used to reconstruct the image through the inverse Fourier transform. Finally, the new augmented data are used to train the artificial neural networks.

The performance of the networks during training was observed with the accuracy metric. Also, these models were validated with the validation dataset through the same metric. Finally, all networks were evaluated with the test set under the accuracy, sensitivity, and specificity metrics.

Each network was run on average eight times under the following hyper-parameters:

- Number of epochs: 200.
- Early stopping: Minimum change in the monitored quantity to qualify as an improvement of 0.00001, and 10 epochs with no improvement for shutdown.
- Optimizer: Adadelta.
- Weight initialization: Uniform Glorot.
- Bias initialization: Zeros.

It should be noted that in each run, the data were randomly selected in proportions of 80, 10, and 10% for training,

Algorithm 1: FOURIER data augmentation training

Input: A dataset: Data $\in \mathbb{R}^{n \times r \times c}$
Output: A Network model: Model

```
begin
    Data ← Normalization(Data)
    Training, Validation, Test ← SplitData(Data)

    for i ← 1 to TrainingDataNumber do
        Data1 ← HorizontalFlip(Training)
        Data2 ← VerticalFlip(Training)
        Data3 ← HorizontalVerticalFlip(Training)
        Training ← Add(Training, Data1, Data2, Data3)

        Function FourierAugmentation(Training):
            Amplitude, phase ← FourierTransform(Training) [eq: 1]
            Noise ← GetRandomNoise(Shape(Amplitude))
            NewAmplitude ← Amplitude ⊙ Noise
            New ← InverseFourierTransform(NewAmplitude, phase) [eq: 4]
            return New
        end

        DataAugmentation ← Add(Training, New)

    Model ← TrainingModel(DataAugmentation, Validation)

    ModelEvaluation(Model, Test)

    return Model
```

Fig. 3 – Pseudocode of the algorithm used in the methodology.

validation, and test data, respectively. The splitting was performed in this way due to the small amount of data. Moreover, the strategy is equivalent to cross-validation and guarantees to avoid bias due to data splitting.

The architectures were modeled under the Python programming language, with the main Keras and TensorFlow libraries. The execution was performed on the Colab platform configured with 25 GB of Ram and Tesla T4 GPU. The implemented codes are available to the public in the following GitHub repository (https://github.com/AndresAnayaIsaza/FourierDeepLearningFoot/).

Finally, since the amount of data is small and the evaluation was performed on 10% of data (test data), we proposed to evaluate the best performing network on the whole data set (training, validation, and test), aiming to obtain a description of the network on the entire real data set (no data augmentation).

4. Results

As mentioned above, the research is based on data augmentation based on the new Fourier transform strategy. Fig. 4 shows some examples of synthesized images. In addition, the reference images that were used to generate these new images are also shown. The results are presented for the two cases, the control group, and subjects with diabetes mellitus. In general, the generated images present a similar structure to the original images but have variations in the foot temperature patterns, i.e., in the maximum temperatures of the image. In this sense, the proposed method implies an excellent strategy to generate new images with the two types of cases; however, it should be clarified that, although the images have human inference and resemble the reference cases, this effect might not be relevant for artificial intelligence. Therefore, the validity of the image synthesis would be given by the performance of the networks trained with the new data set

Table 3 has the number of data used to train the models in the four different conditions, i.e., the models trained from zeros, with the proposed method (Fourier), image flipping, and the combination of the two methods. The results show a marked difference in data enhancement using the combination of the two methods, increasing almost an order of magnitude. In other words, the combination of the methods would be an effective solution for the reduced amount of data.

The following section presents the results generated by the models under the different data augmentation techniques. Tables are presented with the scores in percentage values and the graphs with the corresponding fractional values, i.e., with values from 0 to 1. Table 4 shows the three networks' maximum value between the different training with the test data. The values indicate that the ResNet network achieved a perfect accuracy of 100%, which agrees with the sensitivity and specificity of 100%.

Since ResNet50v2 achieved perfect accuracy, Fig. 5 shows the performance for this network only. The figure presents the accuracy as a function of epochs for training (Fig. 5A)

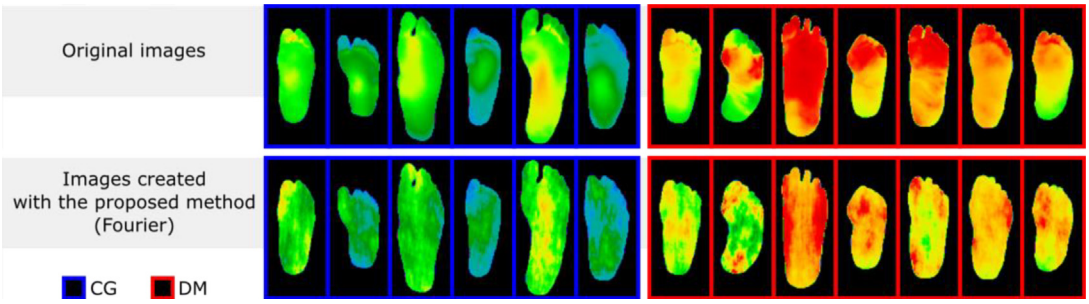


Fig. 4 – Examples of the images synthesized with the magnification of data in the following types of subjects: Control group and Diabetes Mellitus.

Table 3 – Subjects and images used in model training.

Subjects	Thermographs by class	Split of the data*		Number of images in training conditions	
122 DM	244 DM	Training	266	None	266
45 CG	90 CG	Validation	34	Fourier	532
		Test	34	Flip	1064
				Flip & Fourier	2128

* Data were randomized prior to splitting.

Table 4 – Maximum values reached by the models evaluated with the test data.

	Accuracy (%)	Sensitivity (%)	Specificity (%)	FPR* (%)	Data augmentation	
					Flipping	Fourier
ResNet50v2	100	100	100	0	✓	✓
DFTNet	97,06	97,06	97,06	2,94	✗	✓
Transformer	88,24	82,35	88,24	11,76	✗	✗

* False positive rate.

and validation data at each epoch's end (Fig. 5B). Additionally, the model's loss in these two cases, i.e., training and validation, is also presented (Fig. 5C and D). The accuracy converges from epoch 40 for the four cases of data augmentation; however, it can be observed that, for data flipping and data flipping with Fourier, the curves presented a steeper curvature than the other two cases (see Fig. 5A). Similarly, the loss also presented this same behavior for the same two cases (see Fig. 5C), reflecting the network's good performance.

Although the flipping and Fourier flipping methods presented similar behavior during training, the difference is evident in the validation data. The accuracy reached the highest values, indicating no overtraining for the flipping and Fourier data set (See Fig. 5B). The effect is also appreciable with the loss function, where the lowest value was reached (See Fig. 5D).

It should be clarified that the graphs present different lengths since they were implemented with the Early Stopping function, i.e., the models had stopped training when the loss did not have a significant reduction.

Fig. 6 shows the scores obtained with the test data for the three models as a function of the four methods, i.e., without data augmentation, with image flipping, Fourier augmentation, and the combination of the previous two. The eight-training distribution for the accuracy, sensitivity, specificity, and false-positive rate metrics is presented in the figure. Again, the models' high scores for the last case (flipping plus Fourier) show that the networks did not suffer from overtraining. Moreover, the three models presented more homogeneous distributions and higher scores in the three metrics. For example, accuracy showed the smallest boxes and whiskers with high values trends (see Fig. 6A). In Fig. 6A, it is also possible to notice that the ResNet50v2 network presented a better performance than the other two networks. Similarly, ResNet50v2 was above the sensitivity metric (see Fig. 6B). In the case of specificity, the Transformer network presented a marked tendency to high values in the latter case (see Fig. 6C). However, the Transformer presented the worst sensitivity distribution, i.e., the network has a low ability to identify true positives.

Finally, the scores for the untrained case had the worst distributions as expected.

Fig. 7 shows the probability values returned by the network for the two cases (CG and DM). The subjects were organized based on the CG score delivered by the network, and the actual ratings of each subject were included (green dots). It should be clarified that the actual labels have two possible values, i.e., zero or one. However, these were plotted below or above the actual values only to visualize the plots better.

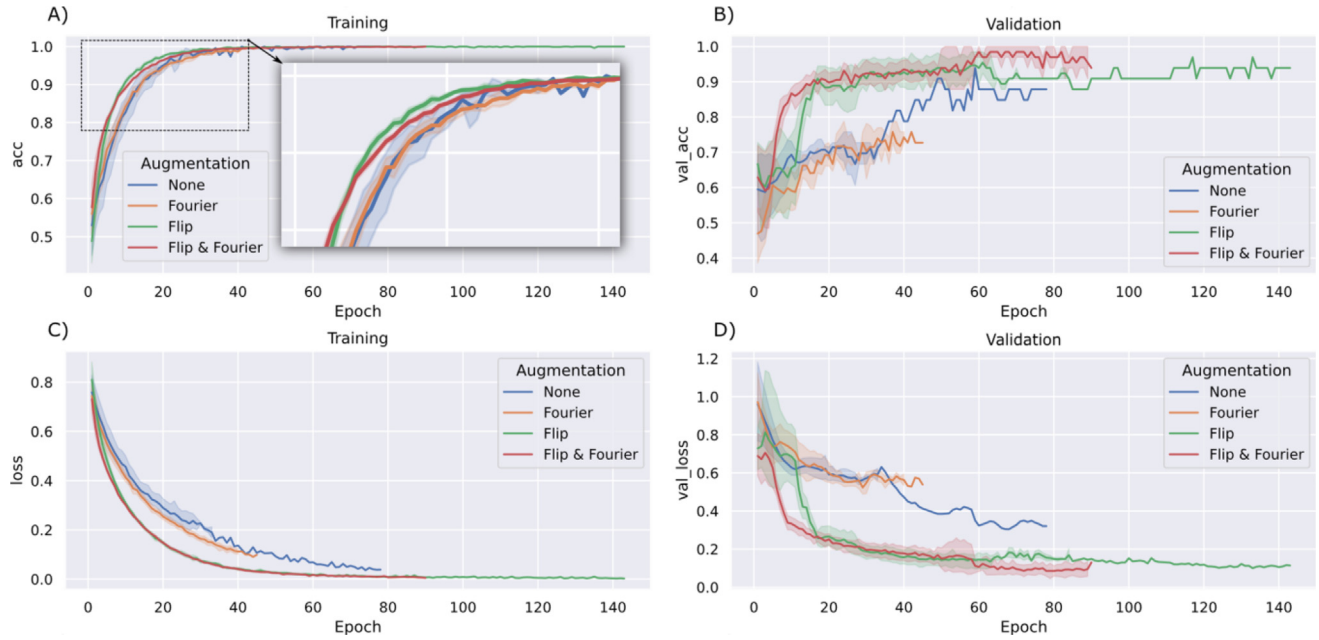


Fig. 5 – ResNet50v2 network training under different data augmentation conditions: A) network accuracy as a function of epochs; B) Model validation at the end of each epoch with validation data; C) Loss of the model as a function of epochs; D) Loss of the validated model with validation data.

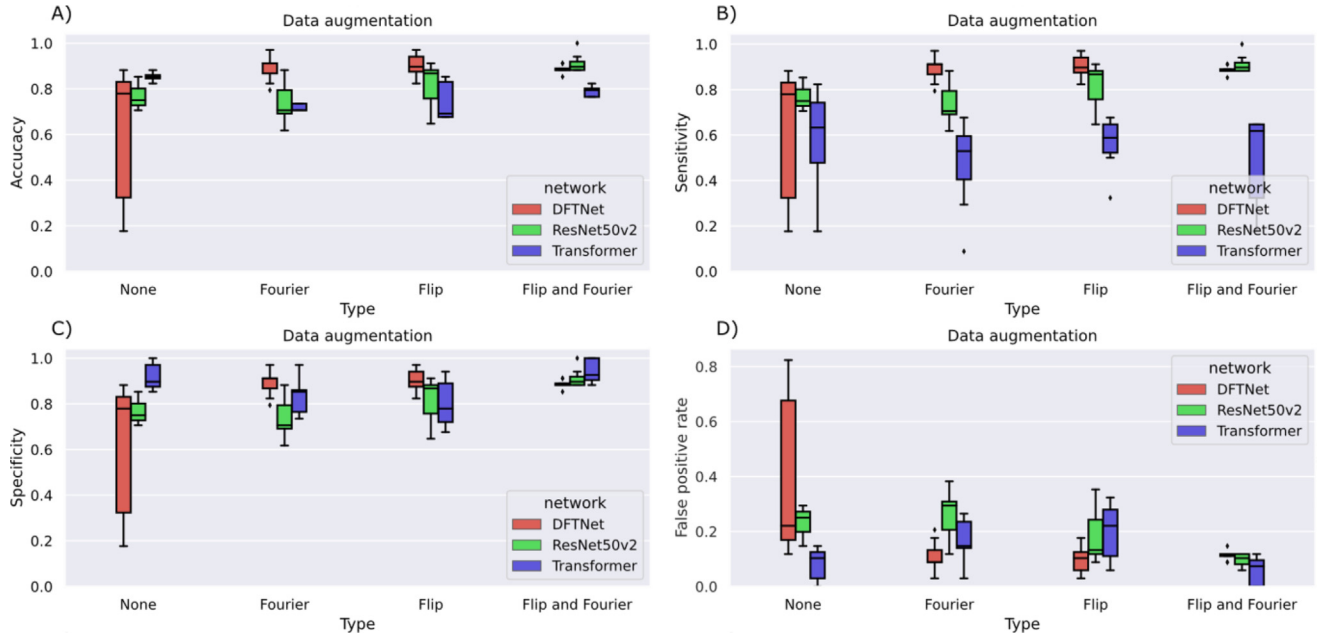


Fig. 6 – Distribution of metrics as a function of the four data augmentation conditions for the three deep learning models: A) accuracy; B) sensitivity; C) specificity; D) false-positive rate. The distributions were generated with the test data.

In Fig. 7A, the ResNet50v2 network classification for the right foot is shown. The network correctly classified all available subjects and presented little uncertainty (probabilities close to zero or one) with a small number of subjects. Similarly, the classification with the left foot had a similar behavior (Fig. 7B); however, the left foot generated two misclassifications, where the misclassified subjects had probability scores of 0.581 and 0.464 (CG output values), these being diabetic and control, respectively. Finally, averaging the network outputs' values between the two feet obtained the classification in Fig. 7C. The classification was perfect, and most subjects were classified with low uncertainty. There were no scores between the values of 0.4 and 0.6.

Finally, Fig. 8 shows some examples of healthy and diabetic subjects with the classification probability generated by the ResNet50v2 network. The figure shows the probability

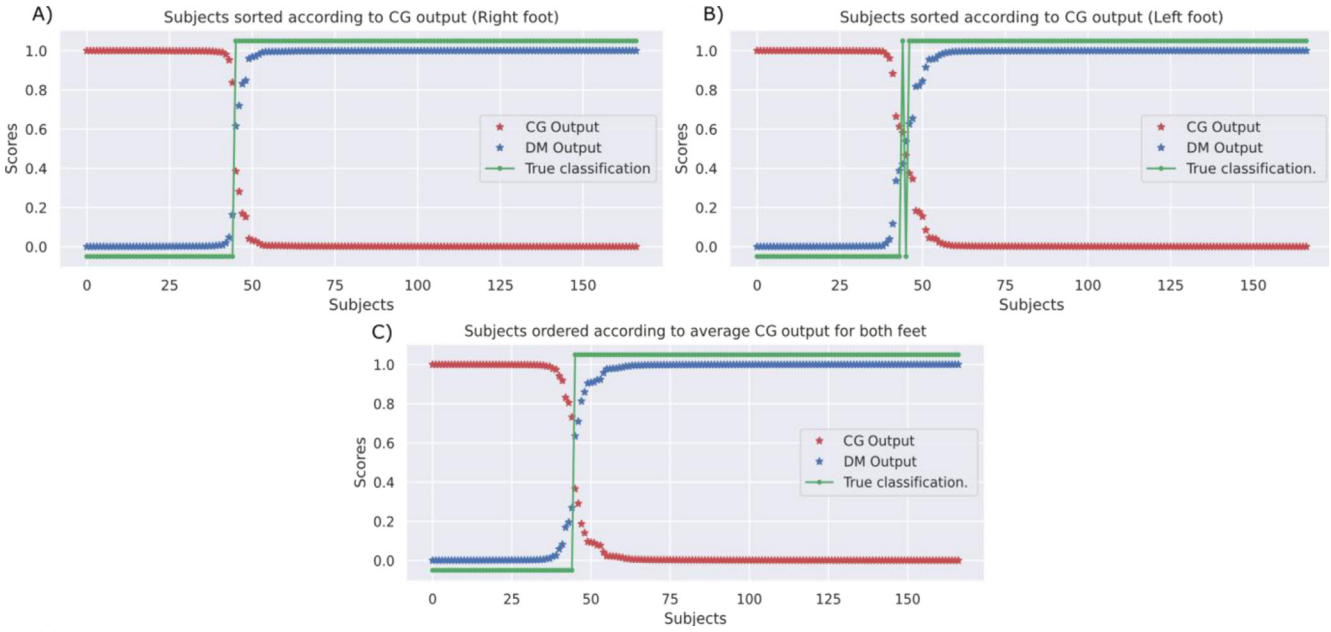


Fig. 7 – ResNet50 network classification with all subjects available and organized according to the probability values of the control group output with the respective true labels: A) Subjects organized with the scores of the right foot; B) Subjects organized with the scores of the left foot; C) Subjects organized with the average scores of both feet.

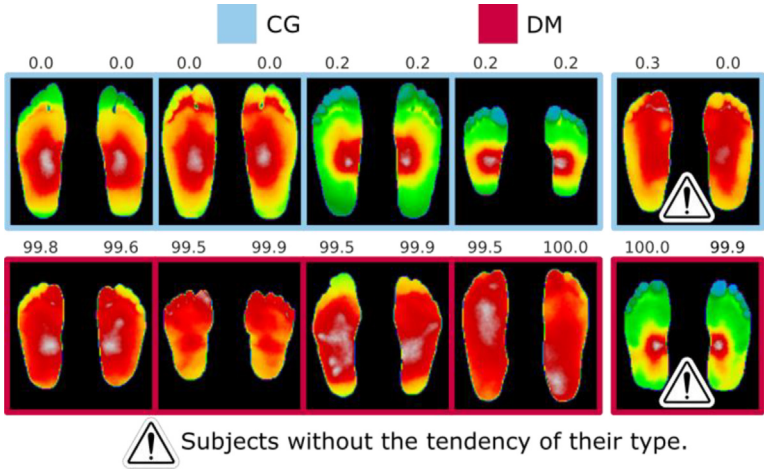


Fig. 8 – Examples of subjects and their probability of belonging to the DM group. The probability is given for each foot and located on the top of each foot.

of belonging to the diabetic group, i.e., the DM output network's probability. Although the results largely agree with the theoretical part, confirming that healthy subjects have a temperature distribution known as a butterfly pattern [63], this is not a determining criterion since some healthy subjects do not have such a pattern (see Fig. 8). Furthermore, from a theoretical point of view, neuropathic diabetic feet present temperature changes mainly due to the increased flow of the arteriovenous shunt, generating irregular patterns in temperature. However, this is not a determining criterion either, since subjects can be found who preserve the butterfly pattern despite having DM, as shown in one of the examples in Fig. 8. The patterns generated by all the subjects are shown in the appendices section to have a global view of patterns.

5. Discussion

Diabetes Mellitus can manifest itself through different pathologies, even triggering the pathogenesis of ulceration in distal extremities. The disease presents severe complications in the subject who suffers from it, leading to amputation of the extremities. In this sense, the detection of diabetic foot is a primordial necessity to avoid future affections. Therefore, in this paper, we proposed to study deep

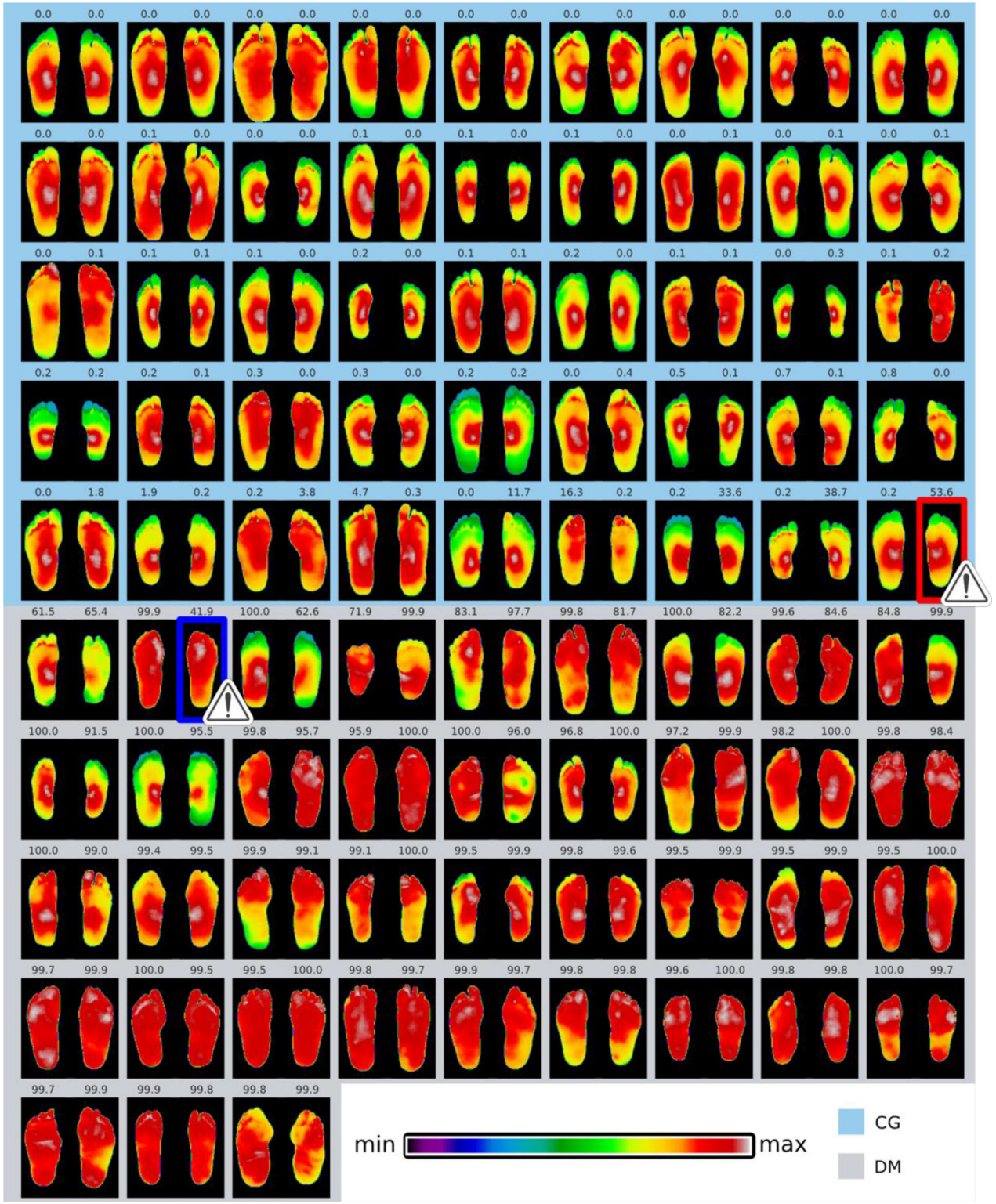


Fig. A9 – Temperature distribution visualization for subjects with the probability of belonging to DM group, the probability is given for each foot and located at the top of each one. The foot framed with the red box is a control subject (healthy) misclassified as DM. The foot framed with the blue box is a DM subject misclassified as healthy.

learning techniques to classify plantar temperature distributions in healthy (CG) and diabetic (DM) subjects.

In contrast to most developments (based on asymmetric analysis), this study was approached as an independent analysis of lower extremity temperature. Furthermore, due to the limited amount of foot thermography data, three data augmentation conditions were used, where a new method based on image modification through amplitude modification in the

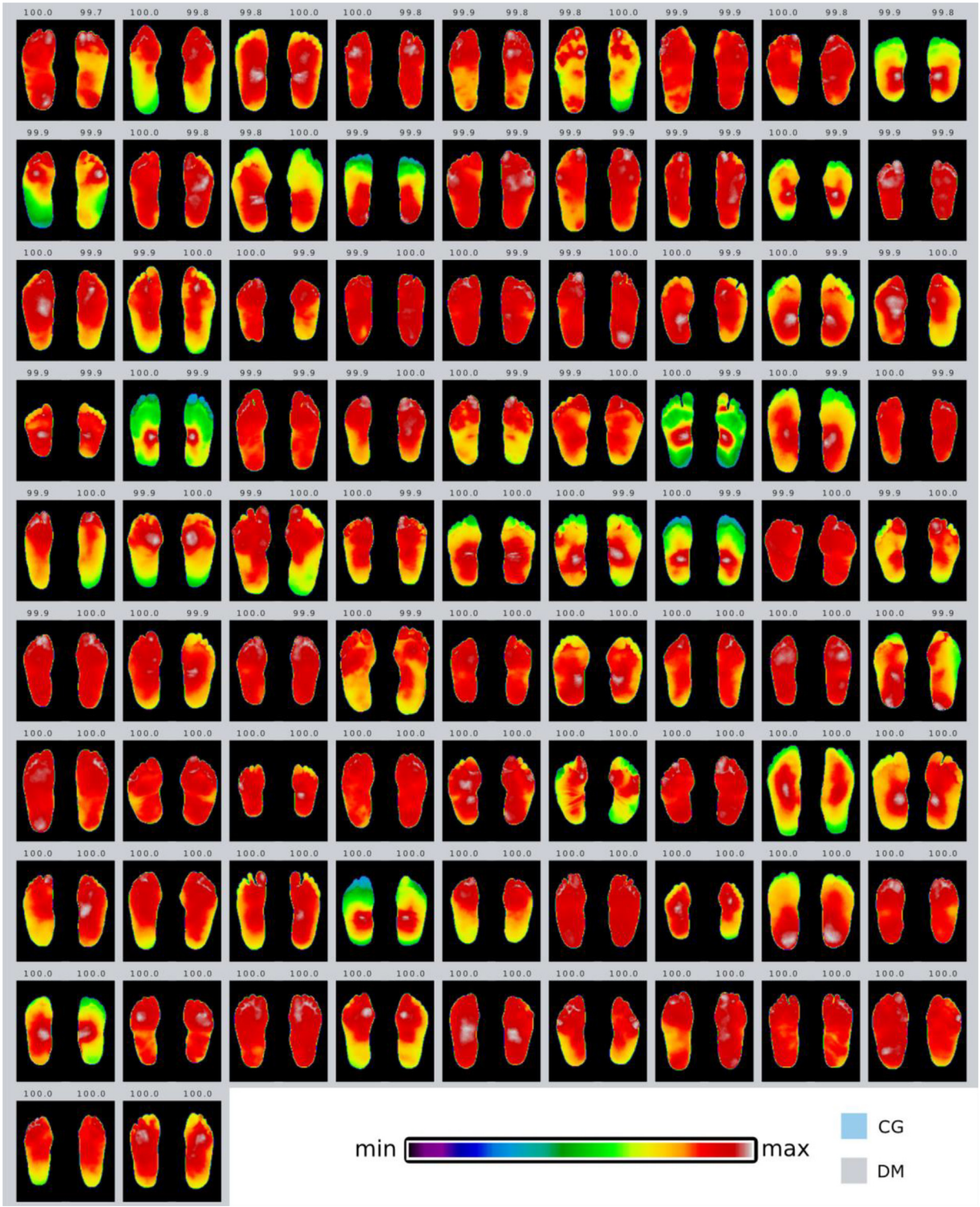


Fig. A10 – Temperature distribution visualization for subjects with the probability of belonging to DM group, the probability is given for each foot and located at the top of each foot.

Fourier transform was proposed. The results showed a better performance with our method together with image flipping. The process allowed to increase the data set; moreover, since there was no evidence of over-training, it is possible to assume that the effect generated by the Fourier transform introduced variability in the images while preserving the fundamental characteristics for the classification of the data. Besides, the original thermograms were clipped around the sole, i.e., all pixels outside this region have zero value. In this sense, although the images with the proposed method modify the background, it could be assumed that this modification is not significant since the method is based on partial magni-

tude alteration; consequently, the background values will remain low despite the modification (see Fig. 2).

Although the training with the different data augmentation methods presented little difference (see Fig. 5), the significant contribution was observed directly with the test data, having greater validity since they are evaluated with data that did not intervene in the training. Therefore, the new data augmentation method with the Fourier transform is presented as a novel and helpful technique in developments with insufficient data. While the proposed method results are promising, some future work is needed to determine precisely how the proposed method acts on the networks. In principle, we assume that altering the amplitude in frequency (Fourier) space partially preserves the temperature distribution. Therefore, the spatial distribution would preserve the subject's nature, i.e., controls or DM. However, we are also including a random element, which could be functioning as a regularization method in the network.

Additionally, we used the DFTNet model, and two architectures based on ResNet50 and Transformers, respectively. The ResNet50 network with our proposed method allowed us to reach a perfect classification of 100% and, although it is not very common to reach this type of result, this may be mainly possible due to the marked difference between control and diabetic subjects. Furthermore, in this specific case, the data set is small, limiting the finding of atypical subjects that could generate confusion in the network. However, it is necessary to take this limitation into account for future work, where it would be necessary to validate the network with a test group and corroborate that the network's performance is maintained at 100% or, failing that, that there is no significant reduction. On the other hand, the results in Table 4 clearly show no overtraining in the models since the scores were obtained with the test data, i.e., with data that did not intervene during training.

On the other hand, it is worth noting that Cruz et al. [48] designed the DFTNet network, outperforming basic machine learning techniques, i.e., they compared it with a multilayer perceptron, a support vector machine (SVM), and even with AlexNet and GoogLeNet, where they demonstrated that the proposed network had generated the highest classification accuracy up to that time. However, the ResNet50 network, with our proposed method, outperformed the scores recorded so far. Moreover, in contrast to conventional machine learning techniques, deep learning methods do not require complex feature extraction methods, as they can find patterns in the complexity of raw data, as seen in this development.

Finally, it was chosen to classify the subjects based on the average scores in both feet, generating a perfect classification with little uncertainty, i.e., no scores between 0.4 and 0.6 were generated. The result is of great utility, as it could be used to identify atypical subjects with values in this range. Additionally, this behavior again reflects the proposed network's high effectiveness for the classification of subjects with diabetic foot.

6. Conclusions

It was proposed to implement three deep learning architectures under three data augmentation methods, where a new method based on the modification of the amplitude of the images, under the Fourier transform, was included. Two convolutional neural networks and a new approach with attention models, known as Transformer, were included in the study. The Fourier method and image flipping augmentation allowed the highest performances to be achieved in the three implemented networks, i.e., DFTNet, ResNet50v2, and Transformer networks. The networks achieved values above 95%, and even a perfect score of 100% was reached through the ResNetv2 network without presenting overtraining. Besides, the architecture presented few subjects with uncertain probabilities, i.e., with low probability that prevented them from being classified in either of the two groups. Also, the network allowed creating an uncertainty threshold of up to 20%, i.e., there were no subjects with intermediate values between 0.4 and 0.6%, ensuring high classification efficiency.

On the other hand, the architecture was able to discriminate between healthy and DM subjects, although the patterns between groups showed variations that could be associated with the opposite group, i.e., the network was able to extract abstract characteristics specific to each group, achieving high classification effectiveness.

Finally, the architecture was designed to classify each foot separately; hence, by taking the average of the probabilities between the two feet, the effectiveness of the network was increased, reaching a perfect classification of 100%, surpassing all existing classification methods and presenting itself as an excellent tool for the discrimination of thermographic images of the diabetic foot.

7. Information sharing statements

The dataset used in this paper is a contribution from Plantar Thermogram Database for the Study of Diabetic Foot Complications Dataset (https://ieee-dataport.org/open-access/plantar-thermogram-database-study-diabetic-foot-complications). The program source code developed in this manuscript is publicly available here (https://github.com/AndresAnayaIsaza/FourierDeepLearningFoot/). For assistance with running the program, please feel free to contact us.

CRediT authorship contribution statement

Andrés Anaya-Isaza: Conceptualization, Methodology, Software, Validation, Formal analysis, Investigation, Resources, Writing – original draft, Writing – review & editing, Visualization, Supervision, Project administration, Funding acquisition. **Martha Zequera-Diaz:** Conceptualization, Resources, Writing – review & editing, Supervision, Project administration, Funding acquisition.

Declaration of Competing Interest

The authors declare that they have no known competing financial interests or personal relationships that could have appeared to influence the work reported in this paper.

Acknowledgements

This research was supported by the research division from BASPI FOOTLAB (https://ingenieria.javeriana.edu.co/investigacion/laboratorio-footlabb) and INDIGO Technologies (https://indigo.tech/).

Appendix A

In this appendix, ResNet50v2 network DM output probability for all subjects, i.e., the probability that the foot belongs to a subject with diabetes mellitus, is given. The subjects are in the same order as in Fig. 6C, but the scores are given for each foot individually (See Fig. A9 and Fig. A10).

REFERENCES

[1] Federación-Internacional-de-Diabetes. Atlas de la diabetes 2019. https://www.diabetesatlas.org/upload/resources/material/20200302_133352_2406-IDF-ATLAS-SPAN-BOOK.pdf (accessed October 8, 2021).
[2] World Health Organization. Diabetes n.d. https://www.who.int/news-room/fact-sheets/detail/diabetes (accessed October 8, 2021).
[3] Cho NH, Shaw JE, Karuranga S, Huang Y, da Rocha Fernandes JD, Ohlrogge AW, et al. IDF Diabetes Atlas: Global estimates of diabetes prevalence for 2017 and projections for 2045. Diabetes Res Clin Pract 2018;138:271–81.
[4] Ingaramo RA. Obesity, diabetes, and other cardiovascular risk factors in native populations of South America. Curr Hypertens Rep 2016;18:9. https://doi.org/10.1007/s11906-015-0613-6.
[5] Egan AM, Dinneen SF. What is diabetes? Med (United Kingdom) 2014;42:679–81. https://doi.org/10.1016/j.mpmed.2014.09.005.
[6] French EK, Donihi AC, Korytkowski MT. Diabetic ketoacidosis and hyperosmolar hyperglycemic syndrome: Review of acute decompensated diabetes in adult patients. BMJ 2019;365. https://doi.org/10.1136/bmj.l1114.
[7] Einarson TR, Acs A, Ludwig C, Panton UH. Prevalence of cardiovascular disease in type 2 diabetes: a systematic literature review of scientific evidence from across the world in 2007–2017. Cardiovasc Diabetol 2018;17:83. https://doi.org/10.1186/s12933-018-0728-6.
[8] Gerstein HC. Diabetes: Dysglycaemia as a cause of cardiovascular outcomes. Nat Rev Endocrinol 2015;11:508–10. https://doi.org/10.1038/nrendo.2015.118.
[9] Harding JL, Pavkov ME, Magliano DJ, Shaw JE, Gregg EW. Global trends in diabetes complications: a review of current evidence. Diabetologia 2019;62:3–16. https://doi.org/10.1007/s00125-018-4711-2.
[10] Bonaca MP, Nault P, Giugliano RP, Keech AC, Pineda AL, Kanevsky E, et al. Low-density lipoprotein cholesterol lowering with evolocumab and outcomes in patients with peripheral artery disease: insights from the FOURIER trial (further cardiovascular outcomes research with PCSK9 inhibition in subjects with elevated risk). Circulation 2018;137:338–50.
[11] Woody J. Overview of diabetic foot care for the nurse practitioner. J Nurse Pract 2020;16:28–33. https://doi.org/10.1016/j.nurpra.2019.08.011.
[12] Bandyk DF. The diabetic foot: pathophysiology, evaluation, and treatment. Semin Vasc Surg 2018;31:43–8. https://doi.org/10.1053/j.semvascsurg.2019.02.001.
[13] Petrova NL, Donaldson NK, Tang W, MacDonald A, Allen J, Lomas C, et al. Infrared thermography and ulcer prevention in the high-risk diabetic foot: data from a single-blind multicentre controlled clinical trial. Diabet Med 2020;37(1):95–104.
[14] Chastain CA, Klopfenstein N, Serezani CH, Aronoff DM. A clinical review of diabetic foot infections. Clin Podiatr Med Surg 2019;36:381–95. https://doi.org/10.1016/j.cpm.2019.02.004.
[15] Rossboth S, Lechleitner M, Oberaigner W. Risk factors for diabetic foot complications in type 2 diabetes—A systematic review. Endocrinol Diabetes Metab 2021;4. https://doi.org/10.1002/edm2.175.
[16] Polk C, Sampson MM, Roshdy D, Davidson LE. Skin and soft tissue infections in patients with diabetes mellitus. Infect Dis Clin North Am 2021;35:183–97. https://doi.org/10.1016/j.idc.2020.10.007.
[17] Ananian CE, Dhillon YS, Van Gils CC, Lindsey DC, Otto RJ, Dove CR, et al. A multicenter, randomized, single-blind trial comparing the efficacy of viable cryopreserved placental membrane to human fibroblast-derived dermal substitute for the treatment of chronic diabetic foot ulcers. Wound Repair Regen 2018;26(3):274–83.
[18] Peter-Riesch B. The diabetic foot: the never-ending challenge, n.d., p. 108–34. 10.1159/000439409.
[19] Ingelfinger JR, Armstrong DG, Boulton AJM, Bus SA. Diabetic foot ulcers and their recurrence. N Engl J Med 2017;376:2367–75. https://doi.org/10.1056/NEJMra1615439.
[20] Bus SA, Waaijman R, Arts M, de Haart M, Busch-Westbroek T, van Baal J, et al. Effect of custom-made footwear on foot ulcer recurrence in diabetes: a multicenter randomized controlled trial. Diabetes Care 2013;36:4109–16. https://doi.org/10.2337/dc13-0996.
[21] Veves A, Murray HJ, Young MJ, Boulton AJ. The risk of foot ulceration in diabetic patients with high foot pressure: a prospective study. Diabetologia 1992;35:660–3. https://doi.org/10.1007/BF00400259.
[22] Bus SA, Armstrong DG, van Deursen RW, Lewis JEA, Caravaggi CF, Cavanagh PR. IWGDF guidance on footwear and offloading interventions to prevent and heal foot ulcers in patients with diabetes. Diabetes Metab Res Rev 2016;32(Suppl 1):25–36. https://doi.org/10.1002/dmrr.2697.
[23] Agrawal K, Chauhan N. Pressure ulcers: back to the basics. Indian J Plast Surg 2012;45:244–54. https://doi.org/10.4103/0970-0358.101287.
[24] Coleman S, Nixon J, Keen J, Wilson L, McGinnis E, Dealey C, et al. A new pressure ulcer conceptual framework. J Adv Nurs 2014;70(10):2222–34. https://doi.org/10.1111/jan.12405.
[25] Dealey C, Brindle CT, Black J, Alves P, Santamaria N, Call E, et al. Challenges in pressure ulcer prevention. Int Wound J 2015;12:309–12. https://doi.org/10.1111/iwj.12107.
[26] Pieper B. Pressure ulcers: impact, etiology, and classification, 2010.
[27] Yavuz M, Ersen A, Hartos J, Lavery LA, Wukich DK, Hirschman GB, et al. Temperature as a causative factor in diabetic foot ulcers: A call to revisit ulceration pathomechanics. J Am Podiatr Med Assoc 2019;109:345–50. https://doi.org/10.7547/17-131.
[28] Bharara M, Cobb JE, Claremont DJ. Thermography and thermometry in the assessment of diabetic neuropathic foot: A case for furthering the role of thermal techniques. Int J Low Extrem Wounds 2006;5:250–60. https://doi.org/10.1177/1534734606293481.

[29] Ilo A, Romsi P, Mäkelä J. Infrared thermography and vascular disorders in diabetic feet. J Diabetes Technol 2019;14:28–36. https://doi.org/10.1177/1932296819871270.
[30] Bouzida N, Bendada A, Maldague XP. Visualization of body thermoregulation by infrared imaging. J Therm Biol 2009;34:120–6. https://doi.org/10.1016/j.jtherbio.2008.11.008.
[31] Ilo A, Romsi P, Mäkelä J. Infrared thermography as a diagnostic tool for peripheral artery disease. Adv Skin Wound Care 2020;33:482–8.
[32] Lahiri BB, Bagavathiappan S, Jayakumar T, Philip J. Medical applications of infrared thermography: A review. Infrared Phys Technol 2012;55:221–35. https://doi.org/10.1016/j.infrared.2012.03.007.
[33] Bandalakunta Gururajarao S, Venkatappa U, Shivaram JM, Sikkandar MY, Al Amoudi A. Chapter 4 - Infrared thermography and soft computing for diabetic foot assessment. In: Dey N, Borra S, Ashour AS, Shi FBT-ML in B-SA and DI, editors., Academic Press; 2019, p. 73–97. 10.1016/B978-0-12-816086-2.00004-7.
[34] Fujita H. AI-based computer-aided diagnosis (AI-CAD): the latest review to read first. Radiol Phys Technol 2020;13:6–19. https://doi.org/10.1007/s12194-019-00552-4.
[35] Ravi D, Wong C, Deligianni F, Berthelot M, Andreu-Perez J, Lo B, et al. Deep learning for health informatics. IEEE J Biomed Heal Informatics 2017;21(1):4–21.
[36] Liu W, Wang Z, Liu X, Zeng N, Liu Y, Alsaadi FE. A survey of deep neural network architectures and their applications. Neurocomputing 2017;234:11–26. https://doi.org/10.1016/j.neucom.2016.12.038.
[37] He K, Zhang X, Ren S, Sun J. Delving deep into rectifiers: Surpassing human-level performance on imagenet classification. In: Proc. IEEE Int. Conf. Comput. Vis., vol. 2015 Inter, 2015, p. 1026–34. 10.1109/ICCV.2015.123.
[38] Castiglioni I, Rundo L, Codari M, Di Leo G, Salvatore C, Interlenghi M, et al. AI applications to medical images: From machine learning to deep learning. Phys Medica 2021;83:9–24.
[39] Faust O, Rajendra Acharya U, Ng EYK, Hong TJ, Yu W. Application of infrared thermography in computer aided diagnosis. Infrared Phys Technol 2014;66:160–75. https://doi.org/10.1016/j.infrared.2014.06.001.
[40] Suissa S, Ernst P. Optical illusions from visual data analysis: Example of the New Zealand asthma mortality epidemic. J Clin Epidemiol 1997;50:1079–88. https://doi.org/10.1016/S0895-4356(97)00158-3.
[41] Adam M, Ng EYK, Tan JH, Heng ML, Tong JWK, Acharya UR. Computer aided diagnosis of diabetic foot using infrared thermography: A review. Comput Biol Med 2017;91:326–36. https://doi.org/10.1016/j.compbiomed.2017.10.030.
[42] Mori T, Nagase T, Takehara K, Oe M, Ohashi Y, Amemiya A, et al. Morphological pattern classification system for plantar thermography of patients with diabetes. J Diabetes Technol 2013;7(5):1102–12.
[43] Liu C, van Netten JJ, van Baal JG, Bus SA, van der Heijden F. Automatic detection of diabetic foot complications with infrared thermography by asymmetric analysis. J Biomed Opt 2015;20:026003. 10.1117/1.jbo.20.2.026003.
[44] Adam M, Ng EYK, Oh SL, Heng ML, Hagiwara Y, Tan JH, et al. Automated characterization of diabetic foot using nonlinear features extracted from thermograms. Infrared Phys Technol 2018;89:325–37.
[45] Carlos Padierna L, Fabián Amador-Medina L, Olivia Murillo-Ortiz B, Villaseñor-Mora C. Classification method of peripheral arterial disease in patients with type 2 diabetes mellitus by infrared thermography and machine learning. Infrared Phys Technol 2020;111. https://doi.org/10.1016/j.infrared.2020.103531 103531.
[46] J JS, Prakash KVMV, Sai GA, Vinod B, Chellappan K. Classification of foot thermograms using texture features and support vector machine. In: Second Int. Conf. Electron. Sustain. Commun. Syst., IEEE; 2021, pp. 1445–9. 10.1109/ICESC51422.2021.9532777.
[47] Hernandez-Contreras D, Peregrina-Barreto H, Rangel-Magdaleno J, Ramirez-Cortes J, Renero-Carrillo F. Automatic classification of thermal patterns in diabetic foot based on morphological pattern spectrum. Infrared Phys Technol 2015;73:149–57. https://doi.org/10.1016/j.infrared.2015.09.022.
[48] Cruz-Vega I, Hernandez-Contreras D, Peregrina-Barreto H, de J, Rangel-Magdaleno, Ramirez-Cortes JM. Deep learning classification for diabetic foot thermograms. Sensors 2020;20. https://doi.org/10.3390/s20061762.
[49] Khandakar A, Chowdhury MEH, Ibne Reaz MB, Md Ali SH, Hasan MA, Kiranyaz S, et al. A machine learning model for early detection of diabetic foot using thermogram images. Comput Biol Med 2021;137:104838.
[50] Shorten C, Khoshgoftaar TM. A survey on image data augmentation for deep learning. J Big Data 2019;6:60. https://doi.org/10.1186/s40537-019-0197-0.
[51] Hernandez-Contreras DA, Peregrina-Barreto H, Rangel-Magdaleno JdeJ, Renero-Carrillo FJ. Plantar thermogram database for the study of diabetic foot complications. IEEE Access 2019;7:161296–307.
[52] LeCun Y, Bengio Y, Hinton G. Deep learning. Nature 2015;521:436–44. https://doi.org/10.1038/nature14539.
[53] Erickson BJ. Basic artificial intelligence techniques. Radiol Clin North Am 2021;59:933–40. https://doi.org/10.1016/j.rcl.2021.06.004.
[54] Kuo C-C-J. Understanding convolutional neural networks with a mathematical model. J Vis Commun Image Represent 2016;41:406–13. https://doi.org/10.1016/j.jvcir.2016.11.003.
[55] Chlap P, Min H, Vandenberg N, Dowling J, Holloway L, Haworth A. A review of medical image data augmentation techniques for deep learning applications. J Med Imaging Radiat Oncol 2021;65:545–63. https://doi.org/10.1111/1754-9485.13261.
[56] Haykin S. Multilayer perceptrons. Neural Networks Learn Mach 2009:122–5.
[57] Karhunen J, Raiko T, Cho K. Unsupervised deep learning. Adv Indep Compon Anal Learn Mach 2015:125–42. https://doi.org/10.1016/B978-0-12-802806-3.00007-5.
[58] Lecun Y, Bottou L, Bengio Y, Haffner P. Gradient-based learning applied to document recognition. Proc IEEE 1998;86:2278–324. https://doi.org/10.1109/5.726791.
[59] Krizhevsky A, Sutskever I, Hinton GE. ImageNet classification with deep convolutional neural networks. In: Pereira F, Burges CJC, Bottou L, Weinberger KQ, editors. Adv. Neural Inf. Process. Syst., vol. 25, Curran Associates, Inc.; 2012.
[60] He K, Zhang X, Ren S, Sun J. Deep residual learning for image recognition. 2016 IEEE Conf. Comput. Vis. Pattern Recognit., IEEE; 2016, p. 770–8. 10.1109/CVPR.2016.90.
[61] He K, Zhang X, Ren S, Sun J. Identity mappings in deep residual networks. Comput Vis – ECCV 2016 2016:630–45. 10.1007/978-3-319-46493-0_38.
[62] Vaswani A, Shazeer N, Parmar N, Uszkoreit J, Jones L, Gomez AN, et al. Attention is all you need 2017.
[63] Nagase T, Sanada H, Takehara K, Oe M, Iizaka S, Ohashi Y, et al. Variations of plantar thermographic patterns in normal controls and non-ulcer diabetic patients: Novel classification using angiosome concept. J Plast Reconstr Aesthetic Surg 2011;64:860–6. https://doi.org/10.1016/j.bjps.2010.12.003.